Promotion of tribological and hydrophobic properties of a coating on TPE substrates by atmospheric plasma-polymerization

Elisa Sainz-García[1], Fernando Alba-Elías[1*], Rodolfo Múgica-Vidal[1], Mariola Pantola-Ruiz[2]

[1] Department of Mechanical Engineering. University of La Rioja. c/ Luis de Ulloa 20, 26004 Logroño, La Rioja, Spain.
[2] Materials Science and Engineering Department, IAAB, Materials Performance Group University Carlos III of Madrid, Av. Universidad 30, 28911, Leganés, Madrid, Spain

Accepted Version for publication in Applied Surface Science

Link to publisher version (DOI): https://doi.org/10.1016/j.apsusc.2016.02.186

Published source citation:

Sainz-Garciá, E., Alba-Eliás, F., Múgica-Vidal, R., & Pantoja-Ruiz, M. (2016). Promotion of tribological and hydrophobic properties 1 of a coating on TPE substrates by atmospheric plasma-polymerization. Applied Surface Science, 371, 50-60. https://doi.org/10.1016/J.APSUSC.2016.02.186

Abstract

An APPJ system was used to deposit a coating that combines a low friction coefficient with a high water contact angle (WCA) on a thermoplastic elastomer substrate (TPE) that is used in automotive profiling. The main drawback of this research is that groups that improve the hydrophobicity of the surface worsen its tribological properties. To overcome this, this study explored the use of various mixtures of differing proportions of two precursors. They were a siloxane, aminopropyltriethoxysilane (APTES) that was used to reduce the friction coefficient by its content of SiO_x and a fluorinated compound, (heptadecafluoro-1,1,2,2-tetrahydrodecyl)trimethoxysilane (FLUSI) that was used to improve the water-repellency characteristics, due to the presence of CF_2 long chains. The coatings were characterized by Scanning Electron Microscopy (SEM), Atomic Force Microscopy (AFM), Attenuated Total Reflectance Fourier Transform Infrared Spectroscopy (ATR-FTIR), X-ray Photoelectron Spectroscopy (XPS), dynamic Water Contact Angle (WCA), stability tests and tribological tests. It was found that an increase of the absorbance area under the SiOSi peak and inorganic groups is related to lower friction coefficients. On the other hand, the higher the CF_2 percentage is, the higher the WCA is. The sample that was coated with 25% of FLUSI and 75% of APTES combined the improvements of both functional properties, the friction coefficient and the WCA. It has an average friction coefficient that is (0.530 ± 0.050) 51.5% lower and a WCA that is (θ_{adv}= 119.8º ± 4.75) 4.4% higher than the uncoated TPE sample. A satisfactory stability in humid ambient for twelve months showed a slight decrease of WCA (4.4%) for this sample. The results of this study permit one to realize the effectiveness of using fluorinated precursors to avoid a significant decrease in the WCA when applying a precursor to anti-friction improvement.

Keywords: Friction Coefficient; Hydrophobic; APTES; FLUSI; Atmospheric-Pressure Plasma Jet; Plasma Polymerization

1. INTRODUCTION

The high performance and relatively low cost of elastomer-based materials has led to an increase in their use [1]. Thermoplastic elastomers (TPEs) combine the mechanical properties of vulcanized rubber (softness, flexibility and resilience) with the ease of processing of thermoplastics [2-3]. This enables the production of rubber-like articles using the rapid processing techniques developed by the thermoplastics industry, with properties optimized for the application [3-4]. TPEs are: moderate in cost and light in weight. They have excellent mechanical properties (high elasticity, good flexibility, and toughness), and high resistance to tears and oxidation. In addition, they are hydrophobic in character, possess chemical resistance, offer a wider processing window, and provide an ability to bond with multiple thermoplastics and an excellent price-performance ratio, all of which make them ideal for huge industrial applications [2, 5]. Nowadays, the global TPEs market is one of the most dynamic markets in the world. The diversity of TPEs means that the market now covers a range of different applications, such as in the automotive industry, wire and cable industry, medical applications, engineering, etc. [4-6]. The use of TPEs in the automotive industry represented over 42% of its market during the period of 2011 to 2013 [6]. In particular, TPEs are widely used in the automotive sealing industry to produce components for various automotive parts that are water tight, dust proof and noise proof.

In some areas of the vehicle, in which there is a slippage, such as between the window channels and the glass and the windshield wipers, the TPE must have a low friction coefficient and high hydrophobicity.

With the aim of providing TPE with a low friction coating, the authors have proved SiO_x based-coatings on ethylene propylene diene monomer (EPDM) and TPE substrates with different precursors (tetraethoxysilane –TEOS- and aminopropyltriethoxysilane –APTES-, respectively) that were deposited using different atmospheric pressure plasma jet (APPJ)

systems [7-8] (PlasmaPlus®, Plasmatreat GmbH, Germany and Plasma Spot®, VITO, Belgium, respectively) and achieved low friction coefficients [9-10]. However, the hydrophobic character of these coatings surfaces was noticeably reduced, quantified by measuring the contact angle of water droplets with the surface (WCA), similarly to anti-friction coatings of others works [11-12]. This study explored the use of various mixtures with different proportions of two precursors to enhance both the friction coefficient and the hydrophobicity of the polymer surface. A siloxane, aminopropyltriethoxysilane (APTES) was used to reduce the friction coefficient by its content of SiO_x and a fluorinated compound, (heptadecafluoro-1,1,2,2-tetrahydrodecyl)trimethoxysilane (FLUSI) was used to improve the water-repellency characteristics, due to the presence of CF_2 long chains. Plasma polymerization by an APPJ system is an appropriate method for depositing such coatings. Compared to current methods of coating, APPJ has many advantages: [a] a solvent-free process, [b] a clean process, [c] no need for vacuum equipment, [d] a lower processing costs, [e] easy scalability for industrial on-line processing, [f] moderate substrate temperature and [g] relatively easy control of plasma parameters (plasma power, gas flow…) [1, 13-15]. The objective of this study is to apply an anti-friction coating to a TPE substrate (used in automotive profiling) whose hydrophobicity surface is not reduced significantly.

2. EXPERIMENTAL PROCEDURE

2.1. Materials

A siloxane, aminopropyltriethoxysilane (APTES), to reduce the friction coefficient and a fluorinated compound, (heptadecafluoro-1,1,2,2-tetrahydrodecyl)trimethoxysilane (FLUSI) to improve the hydrophobicity were used as liquid precursors. The chemical structures of these precursors are shown in Fig. 1. The polymer substrates used in this study were TPE (EPDM +

PP) sheets provided by Standard Profile SA (Spain), an automotive sealing factory. The sheets were cut into samples of 100 x 50 x 2 mm.

2.2. Atmospheric pressure plasma jet (APPJ) and the deposition process

The schematic diagram of the Plasma Spot® APPJ set-up for coating samples can be seen in a previous work by these authors [10]. The deposition process was carried out in two steps - the activation phase and the coating phase. During the activation phase, each sample was treated with nitrogen as the ionization gas at a flow rate of 80 slm, without using any precursor to activate the surface. In the coating phase, each sample was coated by a two-pass process. Nitrogen was used as the carrying gas at a flow rate of 1.5 slm. A different mixture of FLUSI and APTES precursors was employed for each sample. Such mixtures are described in Table 1. Throughout this paper, the term -fluorinated coatings- refers to AF_0, AF_{25}, AF_{50} and AF_{75} samples. The process settings during the APPJ deposition, which were the same for all samples, are shown in Table 2.

2.3. Characterization of coatings

2.3.1. Scanning electron microscopy (SEM)

A JEOL JSM-840 Scanning Electron Microscope (SEM) operating at 10-15 kV was used to examine the coating surface morphology. The wear track produced during the tribological test was observed by the use of a HITACHI S-2400 SEM at an operating voltage of 18 kV. Because the samples are non-conductive, samples surfaces were coated with a thin layer of gold using a plasma sputtering apparatus before the SEM examination.

2.3.2. Atomic force microscopy (AFM)

Atomic force microscopy was used to investigate the surface morphology of the samples. AFM data is collected on a Veeco Instrument with a Nanoscope V system. Samples were

measured in taping mode. Surface roughness measurements were based on root mean square (RMS) roughness values.

2.3.3. Film thickness

To determinate the thickness of the coatings, silicon wafers were coated using the same process parameters as for coated samples (Table 2). The samples were fractured by the use of liquid nitrogen. The fractured samples were tilted at an angle of 80° from a horizontal plane inside the SEM chamber before taking the images. The thickness of the coated silicon wafers was assumed to be the same as that of the TPE samples.

2.3.4. Attenuated total-reflectance-Fourier transform infrared spectroscopy (ATR-FTIR)

Attenuated total reflectance-Fourier transform infrared spectroscopy (ATR-FTIR) was used to study the chemical composition of each coating. Spectrums were recorded by a BRUKER IFS 66 FTIR spectrometer with a Specac Golden Gate ATR accessory based on a single bounce diamond prism. Each spectrum was recorded in the 600-4000 cm^{-1} region with a resolution of 2 cm^{-1} and 64 scans. FTIR deconvolutions were undertaken with the aid of the spectrum analysis program PeakFit 4.12 (SPSS Inc.). Each spectrum was fitted with a mixture of Gaussian and Lorentzian functions.

2.3.5. X-ray photoelectron spectroscopy (XPS)

Surface chemical characterization was carried out by X-ray Photoelectron Spectroscopy (XPS). The system used was a Physical Electronics PHI 5700 spectrometer with a multi-channel hemispherical electron analyzer. The base pressure in the UHV analyzing chamber was below 1.33×10^{-7} Pa. Excitation was accomplished via the Mg Kα line (300 W, 15 kV and 1253.6 eV). The high resolution spectrums were registered in the constant analyzer energy mode with 29.35 eV pass energy. The PHI ACCESS ESCA-V8.0C software package

was used for acquisition of the data. Atomic concentration percentages of the characteristic elements were determined from the spectrum after subtracting a Shirley-type background, and taking into account the corresponding area sensitivity factor for every photoelectron line. XPS deconvolutions were undertaken with the same software as used for the FTIR analysis. The observed XPS bands were curve-fitted using a mixed Gaussian-Lorentzian component profile. For the uncoated TPE and A_{100} samples, a value of 285.0 eV for the hydrocarbon C1s core level was used for calibration of the energy scale. For the fluorinated coatings, the spectrum were corrected for the charging effect by setting the -CF_2 component to a binding energy of 291.4 eV.

2.3.6. Dynamic water contact angle (WCA) measurements

The "tilting plate" method was used to measure the advancing and receding contact angles of all the samples. After each sample was adhered to the plane, a 10 µL deionized water drop was dropped on the sample surface by using a micropipette. The sample surface was then slowly tilted from 0º to 90º at a rate of 1º/s. A video for the drop was continuously recorded. All contact angle measurements were performed at ambient temperature. Three measurements were done for each sample.

2.3.7. Stability tests

In order to have a study about the coatings´ stability in humid environment and the durability of the hydrophobic property, samples were aged in air for twelve months. The test chamber was set at 67% of relative humidity and 15ºC. At the beginning and upon completion of the test, the repellency toward water was measured and the ATR-FTIR spectrums were taken for all the samples. Static water contact angles (WCA) based on the sessile drop method were recorded using a commercial Contact Angle System OCA15plus system (Dataphysics, Germany) and SCA200 software. A total of 4-5 drops (3µL/drop) were taken and averaged to

obtain a value that was characteristic of the contact angle for each sample. The ATR-FTIR spectrums were recorded with the abovementioned spectroscope (see section 2.3.4).

2.3.8. Tribological tests

The tribological behavior of the coatings was investigated with a ball on disk tribometer (CSM Instruments). Two tribological tests with two different counterparts were performed for each sample. In the first one a hardened 100Cr6 steel ball (60-62 HRC, 6 mm in diameter) was used as a counterpart and in the second one a glass ball (6 mm in diameter) was used. The friction coefficient was recorded continuously during the test. The normal load applied was 1 N, the radius was 2.5 mm, the sliding speed was 2 cm/s and the total distance was 1000 m.

3. RESULTS AND DISCUSSION

3.1. Thickness, roughness and SEM analysis

The thickness and roughness of all coated samples are illustrated in Fig. 2. Fig. 3 shows SEM images of the uncoated TPE and the coated samples AF_{50} and AF_{75} and A_{100}.

The differences in the thickness and topography of the samples seem to be determined by the APTES percentage in the precursor mixture. NH_2 groups of APTES play an important role in the adhesion enhancement of the coatings on substrates [16-17]. The absence of APTES and, therefore, NH_2 groups is decisive for the AF_0 sample, which possesses the thinnest coating of all coated samples (33 nm). This sample was coated using just FLUSI as a precursor, the molecule of which is mostly fluorocarbons (Fig. 1). Several authors have identified the problem of adhesion of these groups to substrates [18-19]. In this regard, as shown in Fig. 2, the higher the percentage of APTES in the mixture of precursors, the greater is the thickness of the coating. Furthermore, an increment in the APTES percentage results in a decrement of the flash point of the precursor mixture. The flash point of a liquid is that temperature at

which the liquid emits sufficient vapor to form a combustible mixture with air. The flash point of FLUSI is 168º C and the flash point of APTES is 96º C. An increment in the plasma polymerization in the gas phase and a reduction of plasma polymerization in the substrate take place by lowering the flash point of the precursor mixture [20].

In Fig. 3 (a) and (b), one observes a rough and fibrous appearance of the uncoated TPE sample. This sample has a roughness of 328 nm. In Fig. 2 and Fig. 3, the AF_{50} sample shows the smoothest surface of all samples studied (RMS: 180 nm). This suggests that polymerization occurs predominantly in the substrate surface. The polymer film grows by reacting with the monomer fragments that reach the surface [21]. Fig. 3 (e) and (f) show that the surface of the AF_{75} sample has an appearance that is similar to the uncoated TPE surface. The roughness of this sample (RMS: 291 nm) is similar to the uncoated TPE roughness (RMS: 328 nm) (Fig. 2). A much higher level of spherical particles of 100 nm in diameter is observed to cover practically the entire surface in Fig. 3 (f) (white circle). These particles are formed as a result of gas phase plasma reactions [20]. Similar particles are observed on the AF_{50} sample (white circle in Fig. 3 (d)), although the concentration is much lower. In Fig. 3 (g) and (h), a coating formation is clearly visible on the surface of the A_{100} sample. In this case, using just APTES as a precursor, the degree of plasma polymerization in the gas phase is highest resulting in an increase in particle formation. Such particles land on the surface to grow a smooth layer by the van der Merwe growth mechanism [22]. The creation of such a layer leads to a roughness of 205 nm lower than the AF_{75} roughness (RMS: 291 nm). In addition, one can observe cracks (white arrows), which are typical of coatings that use APTES as a precursor [10]. Surface cracking of this sample can be a direct result of the difference in the densities of uncoated TPE and coated samples, which leads to an uneven shrinkage of the rubber material [23]. Some of these cracks can be seen on the surface of the

AF_{75} sample (white arrow in Fig. 3 (f)), and probably are caused by the creation of an emerging layer.

3.2. ATR-FTIR analysis

The ATR-FTIR spectrums of uncoated TPE and coated samples in the region of 600-4000 cm^{-1} are shown in Fig. 4. For purposes of clarity, these spectrums were displaced from their expected locations. Fig. 5 depicts the ATR-FTIR spectrums of uncoated TPE and coated samples that are related to the three main regions: (I) 980-1280, (II) 1500-1800 y (III) 3000-3700 cm^{-1}.

The uncoated TPE spectrum is characterized by various peaks. Three small peaks located at ~721, ~808 and ~840 cm^{-1} are characteristic of CH_2 rocking vibrations. Moreover, the small peaks that appear at ~896, ~973 and ~998 cm^{-1} correspond to C-C asymmetric stretching vibration and CH_3 asymmetric rocking. The peak located at 1164 cm^{-1} is characteristic of CH_3 asymmetric rocking, C-H wagging vibrations and C-C asymmetric stretching. Finally, the peaks at ~1303, ~1377, ~1460 cm^{-1} are related to the CH_2 wagging vibration, the asymmetric stretching mode of $-CH_3$ and the scissoring vibration of $-CH_2$ respectively. In addition to the foregoing, there are three main absorption bands. First, the strong band at ~1080 cm^{-1} corresponds to a C-O stretching vibration. A second band in the region of 1500-1800 cm^{-1} is related to two different peaks: the -COOH bond (~1600 cm^{-1}) and the C=O bond (~1700 cm^{-1}). The last band, which consists of three peaks, is situated in the region of 2852-2950 $cm^{-1}$and is attributed to different saturated hydrocarbons [10].

As shown in Fig. 4 and 5, the same peaks that are observed in the characteristic spectrum of the uncoated TPE are also identified in all of the coated samples. However, the coated samples exhibit a noticeable increase of such peaks in the three main regions: (I) 980-1280, (II) 1500-1800 y (III) 3000-3700 cm^{-1}.

In regards to the A_{100} sample, a broad band can be observed in Region (I) that corresponds to the overlapping of five different functional groups: the stretching vibration of Si-O-Si at ~1042 cm^{-1} [10, 24-26], the SiOC ring link at ~1074 cm^{-1} [10], the SiOC open link at ~1115 cm^{-1} [10], the SiOC cage link at ~1172 cm^{-1} [10] and OCH_2CH_3 ~1200 cm^{-1} [10,17,25]. In Region (II), the new adsorption band in the range of 1500-1800 cm^{-1} corresponds to the overlapping of the nitrogen-containing groups (NH_2, NH, C-N, C=N) [15-17,25,27-28] at ~1615 cm^{-1} and the unsaturated double bonds associated C=O stretching vibration [16,23,29-30] at ~1700 cm^{-1}. In Region (III), the new wide band that is located around 3000-3700 cm^{-1} is assigned to the overlapping of OH stretching vibration mode [15,27-28,31] and symmetric and asymmetric NH stretch of amino groups [15,17,25,28]. The existence of OH groups is due both to water when coated samples are exposed to the air humidity following the plasma treatment [10,29,31] and water vapor, which can enter the discharge channel from the air during the plasma polymerization at atmospheric pressure [15]. Besides these regions, a small peak can be identified around ~1419 cm^{-1} that is related to the Si-CH_2 bond [25].

In regard to fluorinated coatings, all spectrums show some absorption bands that are similar to those observed in uncoated TPE and A_{100} spectrums. Moreover, new overlapped peaks can be identified in Regions (I) and (II). In Region (I) CF_x (x = 1, 2 and 3) groups can be identified at three different frequencies: ~1150 cm^{-1} [24,27,32], ~1208 cm^{-1} [23,27,33], and ~1242 cm^{-1} [24,32-33]. In Region (II), the new adsorption band corresponds to C=CF_2 groups [23,33] at ~1700 cm^{-1}.

It has been noted that, for all of the coated samples, the behavior of these regions' bands depends largely on the APTES percentage in the precursor mixture. In order to understand these relationships, a more in-depth study of the bands intensity of Regions (I), (II) and (III) was conducted. The spectrums of Regions (I) and (II) of all of the studied samples were

deconvoluted into their overlapping peaks. The deconvolutions can be seen in Fig. 6 and Fig. 7.

Fig. 8 shows the absorbance area under the peaks related to SiOSi, CFx, C=O, OH and N-groups of all of the coated samples. These peaks are associated with enhancement of tribological properties, hydrophobicity and coating adhesion. Fig. 8 (a) illustrates the absorbance area of the peaks of Region (I) with the APTES percentage. In this Figure, one can observe the increase of the absorption areas of SiOSi groups by increasing the APTES percentage in the mixture of precursors. This could be justified by a greater contribution of SIO groups of APTES than FLUSI. CF_x (x = 1, 2 and 3) groups can be seen at three different frequencies (~1150, 1208 y 1242 cm^{-1}). Thus, the variation of CF_x groups in Fig. 8 (a) is the sum of the absorbance areas of these three peaks, despite the overlapping of CF_x and OCH_2CH_3 of APTES at 1208 cm^{-1}. The lower the percentage of FLUSI (more APTES) in the precursor mixture, the lower is the absorbance area of AF_{25}, AF_{50}, AF_{75} y A_{100} samples. The absorbance area of AF_0 is the lowest of those of the fluorinated samples. This is probably due to the poor adhesion of fluorocarbons to the TPE substrate. Fig. 8 (b) illustrates the absorbance area of the peaks of the Region (II) with the APTES percentage. The higher the APTES percentage, the greater is the absorbance area of N-groups and C=O/C=CF_2 peaks. This is related to amines and dissociation of the amines and the ethoxy radicals of APTES molecule [16]. The coating of the AF_0 sample contains N-groups due to the nitrogen employed during the activation and coating phases. In Fig. 8 (c), one can observe how, as Fig 8 (b), an increase in the APTES percentage results in an increase in the absorbance area of the NH/OH peak. It is known that the APTES molecule contains a NH_2 bond. Therefore, such an increase could be due to the increase in that group, since it is assumed that absorption of OH groups should be similar for all coated samples.

Based on the foregoing, it can be concluded that the SiOSi groups (tribological properties) and NH groups (adhesion) are directly related to the APTES percentage, whereas CF_x groups (hydrophobicity) show an inverse relationship.

3.3. XPS analysis

XPS analysis was used to quantify the elements on the surface of the uncoated TPE and coated samples. Atomic concentrations from survey scans of the coatings show clear differences in the concentrations of chemical groups that were found in the coatings as a function of the APTES percentage.

Fig. 9 shows the atomic compositions (at. %) of all coated samples as a function of the APTES percentage. The uncoated TPE sample has the following atomic composition: C1s of 94.3%, O1s of 4.5% and Si2p of 1.2%. The presence of oxygen is derived from the oxidation that takes place during the transformation of pellets into sheets. The silicon traces are likely caused by cross contamination.

In order to study the likely reaction of the nitrogen used as the plasma gas with the polymer film, a pretreated sample was treated with nitrogen as ionization gas at a flow rate of 80 slm, without using any precursor, by a two-pass process. The atomic composition of the activated sample was the following: C1s of 79.2%, O1s of 16.1 %, Si2p of 1.7% and N1s of 1.6%. If we compared the atomic composition of the uncoated TPE with the activated sample, one can observe, apart from carbon, oxygen and silicon, a small percentage of nitrogen which means that some of the nitrogen from the plasma gas has reached the surface of the TPE.

It can be seen that for the AF_{25}, AF_{50} and AF_{75} samples, the higher the APTES percentage is, the greater are the oxygen, silicon and nitrogen percentages and the lower is the fluorine percentage. Such variations are due to the decrease in the FLUSI percentage in the precursor mixture, since it is FLUSI that provides fluorine to the coatings (Fig. 1). The chemical composition of the AF_0 sample is determined by the absence of the NH_2 groups of APTES.

This absence affects mainly the non-adherence of fluorocarbons to the substrate, since SiO_x groups have inherently good adhesion [34]. Therefore, the atomic percentage of fluorine in this sample is the lowest (F1s: 15.5%) of all fluorinated coatings (AF_{25}: 46.2%, AF_{50}: 39.8% y AF_{75}: 23.1%), whereas the silicon percentage (Si2p: 14.3%) and the oxygen percentage (O1s:23.1 %) have relatively high values. The carbon percentage (C1s: 46.6%) is the highest of that of all the fluorinated coatings (AF_{25}: 33.3%, AF_{50}: 29.8 y AF_{75}: 38.0%). A factor influencing the increase in the C1s percentage may be the low F1s percentage. The nitrogen (N1s: 0.5 %) is derived from the N_2 plasma gas which can react and reach the surface of the film as was explained before. The absence of fluorine in the A_{100} sample is balanced by the increase in carbon (C1s: 60.0%). The oxygen (O1s: 23.3%), silicon (Si2p: 11.8%) and nitrogen (N1s: 3.4%) percentages remain largely the same as in the AF_{75} sample (C1s: 38.0%, O1s: 24.0%, Si2p: 11.9%, N1s: 3.0%, F1s: 23.1%).

In order to study the relationship between the hydrophobicity and the chemical composition of the coatings, C1s spectrums were deconvoluted into the six most representative components that correspond to the main bonding regions. Due to the small differences in energy between some functional groups, it was not possible to get a unique distinction of some peaks [14]. Table 3 shows the assigned chemical components and the peak position in the deconvoluted high resolution C1s spectrum. Representative, deconvoluted, high-resolution, C1s spectrums of all samples are shown in Fig. 10. The C1s spectrum of the uncoated TPE and the A_{100} sample show a main peak at around 285 eV. The deconvolution of these samples is comprised of C-Si, C-H/C-C, C-O/C-N and C=O bonds. Fluorinated coatings, besides the mentioned peak, show a new peak situated at about 291.4 eV, which is related mainly to CF_2 bonds.

Fig. 11 (a) shows the relative percentage of fluorine-containing chemical bonds (components D, E and F) as a function of the APTES percentage. In Fig. 9 and Fig. 11 (a), one can see that

an increment in the APTES percentage results in a similar variation of the fluorine atomic (AF_0: 15.5%, AF_{25}: 46.2%, AF_{50}: 39.8%, AF_{75}: 23.1%) percentage and CF_2 relative percentage (AF_0: 4.3%, AF_{25}: 20.1%, AF_{50}: 12.5%, AF_{75}: 7.5%) for all fluorinated coatings. In the case of AF_{25}, AF_{50}, AF_{75} and A_{100} samples, the higher the APTES percentage is, the higher the C=O/CF relative percentage (AF_{25}: 0.0%, AF_{50}: 1.8%, AF_{75}: 4.7%, A_{100}: 6.7%) is that is due to the decomposition of APTES molecules that produce hydrophilic polar groups like C-O, C=O, C-OH, C-N and NH_2 [17,23,27], which are incorporated in the TPE surface by the plasma-polymerization process. For these reason, the C=O group plays a key role in the composition of the D component. Only AF_0 and AF_{75} samples contain a small percentage of CF_3.

In order to study the relationship between the tribological properties and the chemical composition of the coatings, Si2p spectrums were deconvoluted into the five most representative components that correspond to the main bonding regions. Table 3 shows the assigned chemical components and peak position in the deconvoluted high resolution Si2p spectrum. Representative deconvoluted high resolution Si2p spectrums of all samples are shown in Fig. 12. Fig. 11 (b) shows the relative percentages of components G, H, I, J and the accumulated proportion of G component added to H component and I component added to J component as a function of the APTES percentage. The chemical bonds $(CH_3)_4Si$ (component G), $(CH_3)_3SiO$ (component H) and $(CH_3)_2SiO_2$ (component I), are referred to as the organic nature, and the chemical bonds of CH_3SiO_3 (component J) and SiO_4 (component K) are referred to as the inorganic nature [36]. Some authors associate the inorganic character with the surface hardness of a coating [36-37]. As can be seen in Fig. 11 (b), for AF_{25}, AF_{50}, AF_{75} and A_{100} samples, when the APTES percentage is increased, a high accumulated proportion of chemical bonds CH_3SiO_3 and SiO_4 is obtained (AF_{25}: 7.5%, AF_{50}: 8.8%, AF_{75}: 10.6%, A_{100}:

11.8%). This results in a greater inorganic character and a greater surface hardness of the coatings [36].

3.4. Hydrophobicity

Since the equilibrium contact angle cannot be determined on practical polymer surfaces due to their chemical heterogeneity and surface roughness [38-39], the hydrophobic nature of the surfaces was quantified by measuring the dynamic WCA. In this way, advancing and receding contact angles were measured and the hysteresis, the difference between the advancing and receding contact angles, was calculated. It is well established that the advancing contact angle is more sensitive to the low energy components, like CF_x or CH_x, whereas the receding contact angle is more sensitive to the high energy groups, like polar groups [38-39]. In terms of topography, the advancing and receding contact angles can respond differently to increasing surface roughness. An increase in roughness means an increase of the advancing contact angle and a decrease of the receding one [38].

The surface of the uncoated TPE has a hydrophobic character (θ_{adv}=114.9º; θ_{rec}=77.1º), probably due to the long hydrocarbon chains in the polymer backbone [24]. In addition to this, a certain hysteresis is probably due to the surface roughness of the substrate (RMS: 328 nm). Fig. 13 shows the advancing and receding contact angles, relative percentage of the CF_2 (component E) and relative percentages of the polar groups: C-O/C-N (component C) added to C=O (component D) of the coated samples as a function of the APTES percentage. As mentioned in the XPS analysis, it is believed that the major contribution of D component is attributable mainly to C=O groups. Similar to other studies [14, 24], and as Fig. 13 illustrates, the WCA values, especially the advancing contact angle values, are directly correlated to the relative percentage of CF_2. The higher the CF_2, the higher is the advancing contact angle. It is known that an ideal hydrophobic fluorine-containing polymer surface should have a structure that is based on CF_2 long chains like PTFE [14].

Despite only using a fluorinated compound as precursor, sample AF_0 has a dynamic WCA lower than dynamic WCA of the other fluorinated samples (AF_{25}, AF_{50} and AF_{75}). This situation shows the synergistic effect produced by mixing precursors as FLUSI and APTES. A hypothesis which can justify the abovementioned results would be that an improvement of the adhesion of fluorinated compounds is obtained thanks to the amines produced by the APTES decomposition.

Sample A_{100} has the lowest dynamic WCA of the samples studied. This sample contains the highest relative percentage of hydrophilic polar groups of APTES decomposition. These high energy groups promote a reduction of the contact angles, primarily the receding contact angle [38-39]. For AF_{25}, AF_{50}, AF_{75} and A_{100} samples, the higher is the APTES percentage, the higher is the relative percentage of hydrophilic polar groups (C component added to D component and the lower is the advancing and receding contact angles [1,23,30]. However, this trend is not satisfied for sample AF_{50}, since this sample should have a receding contact angle lower than sample AF_{25}. This could be justified by the low roughness of AF_{50} (RMS: 180 nm), which contribute to a higher receding contact angle for such sample. Therefore, it can be concluded that the hydrophobicity of the coated samples is directly correlated to CF_2 groups and inversely correlated to polar groups.

3.5 Stability tests

Stability and durability are important properties in evaluating further industrial feasibility. Related to the ATR-FTIR spectrums, Figure 14 illustrates the ATR-FTIR spectrums of two regions (Regions I and II) for the most representative samples (uncoated TPE, AF_{25} and AF_{75}) at the beginning and upon completion of the stability test. In Region I (980-1280 cm^{-1}), the decrease in the intensity of the main peak around 1070 cm^{-1} of the uncoated TPE is probably related to the loss of C-O groups for the aging process. It is possible to identify this reduction in the spectrums of AF_{25} and AF_{75} samples. For these samples there is no lessening of the

intensity of peaks related to fluorinated compounds (~1150 and ~1240 cm^{-1}). The absorption band in Region II (1500-1800 cm^{-1}) is practically unchanged for uncoated TPE, whereas for AF_{25} and AF_{75} samples one can note a decrease in the intensity of the peak related to C=O and $C=CF_2$ groups (~1700 cm^{-1}). For AF_{25} sample, this decrease results in the disappearance of the peak. This reduction is likely due to the humid ambient.

Figure 15 shows the static WCA obtained from the stability test performed to all the studied samples. On one hand, the WCA of AF_0 and A_{100} remained unchanged. On the other hand, a decrease in the WCA was produced for uncoated TPE, AF_{25}, AF_{50} and AF_{75} samples. This decrease is more marked for lower APTES percentages. This fact seems to be related with the decrease of the intensity of $C=O/C=CF_2$ peak identified in Figure 14.

3.5. Tribological tests

This section analyzes the relationship between the APTES percentage, the chemical characteristics and the friction coefficient of all of the samples. Table 4 presents the measurements of the average friction coefficient for all samples with both the steel ball and the glass ball as counterpart. These samples were tested by applying 1 N at 2 cm/s for a sliding distance of 1000 m. Fig. 16 illustrates the variation in the friction coefficient with the sliding distance for all the samples tested with the steel ball. In regards to the AF_{25} sample, two different stretches are shown, namely AF_{25} [a] tested during a sliding distance of 22 m and AF_{25} [b] tested during a sliding distance of 1000 m. In order to make them easily visible, these tests are presented in a subfigure that shows the first 25 meters of the tribological tests. SEM micrographs in Fig. 17 show the wear tracks of the uncoated TPE, AF_{25} [a], AF_{25} [b] and A_{100} samples at two different magnifications (x 80 and x 600). Fig. 17 (a), (c), (e) and (g) show the friction zone outlined by dashed lines. Fig. 17 (b), (d) and (f) provide a detailed view that corresponds to the white box in Fig. 17 (a), (c) and (e). Fig. 17 (c) – (f) shows the wear tracks of two stretches of the AF_{25} sample after a sliding distance of 22 m (AF_{25} [a]) and

1000 m (AF_{25} [b]). In Fig. 17 (c) and (d) one can see ridges that formed on the surface of the sample arranged perpendicular to the sliding counterpart movement. These are probably due to delamination wear of both the coating and the surface of the TPE substrate. This wear mechanism seems to be emphasized by hard debris, consisting of SiO_x, which detached from the coating at the beginning of the test. The hard debris results in an increase in the friction coefficient, reaching a maximum value during the running-period. The friction coefficient gradually decreases while the ridges are being removing from the surface of the track that carries the hard debris. Once the ridges and hard debris disappear, a stabilization of the friction coefficient occurs during the steady-state period. During this period the exposed surface consists of worm areas of TPE substrate, coated areas (Fig. 17 (f)) and the soft debris of the remains of ridges (white circles in Fig. 17 (e)). This agrees with the results obtained by others authors who have used polymer substrates [40]. As a result, the surface of the AF_{25} [b] sample (Fig. 17 (e) and (f)) is smoother than that of the AF_{25} [a] sample (Fig. 17 (c) and (d)). It is not possible to see any ridges, but some detachment of the coating adhering to the surface (white arrows in Fig. 17 (f)) can be expected. Most of the wear of the AF_{25} sample takes place at the beginning of the friction test. In Fig. 17 (c) and (e) one can see that the track width after 22 m of sliding distance (22 m: ~ 0.6 mm) represents 60% of the track width reached at the end of the test (1000 m: ~ 1 mm). The absence of hard debris in the wear mechanism of the uncoated TPE sample justifies the non-existence of the maximum peak in the running period of this sample's friction test (Fig. 16). After 1000 m of sliding distance, ridges that originated due to substrate delamination wear can be identified (Fig. 17 (a) and (b)).

In Table 4 and Fig. 16, one can see that the wear mechanism described above for the AF_{25} sample is similar to that of the AF_0 and AF_{50} samples. As mentioned in the XPS analysis, the inorganic character and hardness of the coatings are directly correlated to the APTES percentage. Therefore, the lower the APTES percentage is, the softer the coating is, the higher

the wear is and the faster hard debris form resulting in wear delamination of the surface. This is consistent with the delayed onset of the peak of the friction coefficient tests for the AF_0, AF_{25} and AF_{50} samples. The higher the APTES percentage is, the greater is the delay in the growth of the peak. This wear mechanism is particularly relevant for the AF_0 sample, since the maximum value of its friction coefficient reached in the first 8 m is higher than the uncoated TPE sample average friction coefficient.

The study of AF_{75} and A_{100} samples revels that the wear mechanism identified differs from that mentioned above for AF_0, AF_{25} and AF_{50} samples due to the greater hardness of these coating, which results in a less wear. In the friction coefficient tests of AF_{75} and A_{100} samples (Fig. 16), it was not possible to identify the characteristic peak of AF_0, AF_{25} and AF_{50} samples at the beginning of the test. The greater wear resistance of AF_{75} and A_{100} samples prevents delamination wear and a consequent detachment of hard debris of the coating surface.

The surface of the track of sample A_{100} after a sliding distance of 1000 m can be seen in Fig. 17 (g). In this image, it is possible to observe the typical cracks (white arrows in Fig. 17 (g)) that were identified on the original coating surface (white arrows in Fig. 3 (h)). Therefore, apart from some detachment (white circle in Fig. 17 (g)), most of the original coating has been maintained during the tribological test. In Fig. 16, one can see that the friction coefficient of samples AF_{75} and A_{100} is noticeably lower than those of the remaining coated samples. For these samples, the friction coefficient increases gradually with sliding distance due to the increase in the real area of contact between the steel counterpart and the surface of the coating [41]. This increase is more pronounced for the AF_{75} sample because of the lower hardness of its coating.

Since for a specific application of such coating to window channels, the materials in contact are the windoglass with the TPE sealing, the tribological behavior of all the samples with a glass ball as counterpart were tested. As one can see in Figure 16, Figure 18 and Table 4, the

measurements using a glass ball as counterpart are higher than the ones obtained by using a steel ball. Furthermore, similar relationships between the measurements performed with glass and steel balls were found, that is, the more APTES percentage, the lower friction coefficient. In order to determinate the relationship between: [a] the APTES percentage [b] the chemical structure of the coating, [c] the hydrophobicity character and [d] the average friction coefficient, the most relevant results are provided in Fig. 19. With regard to the average friction coefficient, Fig. 19 (a) and (e) show that the absorbance areas under the SiOSi peak are inversely correlated to the friction coefficient. It may be noted that an increment of SiOSi peak is related to the an improvement of the tribological properties of the coated samples as various works reported in the literature [10,37]. Moreover, in Fig. 19 (b) and (e), for the AF_{25}, AF_{50}, AF_{75} and A_{100} samples, an inverse relationship between the relative percentage of inorganic groups (CH_3SiO_3 added to SiO_4) and the average friction coefficient can be observed. As has been noted already by other authors, the higher proportion of the CH_3SiO_3 and SiO_4 chemical bond provides an increase in the wear resistance of the coating. This leads to a decrement of the friction coefficient [10,36]. In regards to the hydrophobicity, Fig. 19 (c), (d) and (e), for AF_{25}, AF_{50}, AF_{75} and A_{100} samples, the relationship between the advancing WCA and the relative percentage of CF_2 and the relative percentage of polar groups (sum of C-O, C-N and C=O) is positive and negative respectively.

The chemical characteristics of the AF_0 sample depend largely on the fluorocarbons' poor adhesion to the substrate because of the absence of NH groups of the APTES molecule.

In Fig. 19, one can see that the A_{100} sample has the highest values of: [a] SiOSi, [b] polar groups and [c] inorganic groups (regardless of the AF_0 sample) besides a total absence of CF_2, which seem to justify both the lowest average friction coefficient (0.461 ± 0.015) and advancing WCA ($89.0^{o} \pm 1.56$). These results confirm that sample A_{100} would perform well in applications in which anti-friction is required, but poorly in water-repellency applications.

However, although the AF_{75} sample has an average friction coefficient (0.530 ± 0.050) that is 14.9% higher than that of the A_{100} sample, its hydrophobic character (θ_{adv} = 119.8º ± 4.75) is 25.7% greater. This is why the AF_{75} sample satisfies the main objectives of this work. It possesses optimal values in both friction coefficient and hydrophobicity at the same time, although such values were not the best values of all samples that were studied.

4. CONCLUSIONS

An APPJ system was used to deposit a coating that combines a low friction coefficient with a high WCA. In order to satisfy this objective, several mixtures with different proportions of APTES and FLUSI were tested.

As a result of the studies and analysis, it was discovered that there is a clear relationship between: [a] the functional properties of the coating (friction coefficient and hydrophobicity), [b] the absorbance area under SiOSi peak, [c] the relative percentage of inorganic groups, [c] the relative percentage of CF_2 and [d] the relative percentage of polar groups as a function of the APTES percentage in the precursor mixture.

In view of the AF_0 sample characteristics, it can be stated that NH groups must be provided to the coatings to ensure that the fluorocarbons of the fluorinated precursor adhere to the substrate. In this paper, the APTES precursor is responsible for providing the NH groups.

The A_{100} sample has an average friction coefficient (0.461 ± 0.015) and an advancing WCA (89.0º ± 1.56), which is 57.5% and 22.5% lower respectively than that of the uncoated TPE sample (CoF: 1.084 ± 0.019 and θ_{adv}: 114.9º ± 5.27). The AF_{75} sample has an average friction coefficient (0.530 ± 0.050) 51.5% lower and an advancing WCA (119.8º ± 4.75) 4.4% higher than the uncoated TPE sample. Taking into account the little difference in the improvement percentage of the friction coefficient values for samples AF_{75} and A_{100} and the low WCA of the A_{100} sample with respect to the uncoated TPE sample, one can conclude that the AF_{75} sample combines the improvement in both functional properties, which were the aim of this

work. In addition, this sample shows a good behavior in the stability test, since its chemical nature has remained unchanged, so that its WCA has just decreased in 4.4% for one year. It is worth underscoring the effectiveness of using fluorinated precursors as FLUSI to avoid a significant decrease in the WCA of the surface of samples when applying a precursor (APTES) to anti-friction improvement. However, the fluorinated precursor proportion used in the mixtures should not exceed 25% to avoid significant deterioration of the tribological properties of the coatings.

In future research, the authors will study the lowest FLUSI percentage to use in the mixture to significantly reduce the friction coefficient, while maintaining the hydrophobicity character. Other precursors (silanes and fluorocarbons) will be explored in order to improve both the friction coefficient and the WCA achieved in this work with APTES and FLUSI.

Acknowledgments

This work was funded by the Regional Research Plan of the Autonomous Community of La Rioja (Spain) through project FOMENTA 2010/02.

References

[1] A. Bismarck, W. Brostow, R. Chiu, H.E. Hagg Lobland, K.K.C. Ho, Effects of surface plasma treatment on tribology of thermoplastic polymers, Polym. Eng. Sci. (2008) 1971-1976.

[2] R. Elleuch, K. Elleuch, B. Salah, H. Zahouani, Tribological behavior of thermoplastic polyurethane elastomers, Mater. Des. 28 (2007) 824-830.

[3] G. Holden, Thermoplastic elastomers, Appl. Plas. Eng. Handbook. (2011) 77.

[4] T. Parenteau, E. Bertevas, G. Ausias, R. Stocek, Y. Grohens, P. Pilvin, Characterisation and micromechanical modeling of the elasto-viscoplastic behavior of thermoplastic elastomer, Mech. Mater. (2013).

[5] S.S. Banerjee, A.K. Bhowmick, Novel nanostructures polyamide 6/fluoroelastomer thermoplastic elastomeric blends: influence of interaction and morphology on physical properties, Polymer. 54 (2013) 6561-6571.

[6] TPE 2012 focuses on end-use applications, Sealing Technology, Vol. 2012, Issue 4 (2012) 6.

[7] J. Ihde, R. Wilken, J. Degenhardt, A. Knospe, C. Buske, WO Patent No. 042459, 6 Oct. 2010.

[8] R.J.M. Rego, D. Havermans, J.J. Cools, WO Patent No. 081637, 6 Feb 2006.

[9] F. Alba-Elías, J. Ordieres-Meré, A. González-Marcos, Deposition of thin-films on EPDM substrate with plasma-polymerized coating, Surf. Coat. Technol. 206 (2011) 234-242.

[10] F. Alba-Elías, E. Sainz-García, A. González-Marcos, J. Ordieres-Meré, Tribological behaviuor of plasma-polymerized aminopropyltriethoxysilane films deposited on thermoplastic elastomers substrates, Thin Solid Films. 540 (2013) 125-134.

[11] J. Chen, J. Wang, H. Yuan, Morphology and performances of the anodic oxide films on Ti6Al4V alloy formed in alkaline-silicate electrolyte with aminopropyl silane addition under low potential, Appl. Surf. Sci. 284 (2013) 900-906.

[12] M. Thieme, F. Streller, F. Simon, R. Frenzel, A.J. White, Superhydrophobic aluminium-based surfaces: wetting and wear properties of different CVD-generated coating types, Appl. Surf. Sci. 283 (2013) 1041-1050.

[13] D. Merche, N. Vandencasteele, F. Reniers, Atmospheric plasmas for thin film deposition: A critical review, Thin Solid Films. 520 (2012) 4219-4236.

[14] G. Borcia, N.M.D. Brown, Hydrophobic coatings on selected polymers in an atmospheric pressure dielectric barrier discharge, J. Phys. D: Appl. Phys. 40 (2007) 1927-1936.

[15] M. Bashir, J. M. Rees, W. B. Zimmerman, Plasma polymerization in a microcapillary using atmospheric pressure dielectric barrier discharge, Surf. Coat. Technol. 234 (2013) 82-91.

[16] C. Volcke, R.P. Gandhiraman, V. Gubala, J. Raj, Th. Cummins, G. Fonder, R.I. Nooney, Z. Mekhalif, G. Herzog, S. Daniels, D.W.M. Arrigan, A.A. Cafolla, D.E. Williams, Reactive amine surfaces for biosensor applications, prepared by plasma-enhanced chemical vapour modification of polyolefin materials, Biosens. Bioelectron. 25(2010) 1875-1880.

[17] M.F.S. Dubreuil, E.M. Bongaers, P.F.A. Lens, Incorporation of amino moieties through atmospheric pressure plasma: Relationship between precursor structure and coating properties, Surf. Coat. Technol. 206 (2011) 1439-1448.

[18] X. Jiang, J. Wang, J. Shen, R. Li, G. Yang, Improvement of adhesion strength and scratch resistance of fluorocarbon thin films by cryogenic treatment, Appl. Surf. Sci. 288 (2014) 44-50.

[19] R.G. Wankhede, S. Morey, A.S. Khanna, N. Birbilis, Development of water-repellent organic-inorganic hybrid sol-gel coatings on aluminium using short chain perfluoro polymer emulsion, Appl. Surf. Sci. 283 (2013) 1051-1059.

[20] C.E. Nwankire, G. Favaro, Q. Duong, D.P. Dowling, Enhancing the mechanical properties of superhydrophobic atmospheric pressure plasma deposited siloxane coatings, Plasma Processes Polym. 2 (2011) 305-315

[21] L. Sandrin, M.S. Silverstein, E. Sacher, Fluorine incorporation in plasma-polymerized octofluorocyclobutane, hexafluoropropylene and trifluoroethylene, Polymer. 42 (2001) 3761-3769.

[22] A. Michelmore, P. Martinek, V. Sah, R.D. Short, K. Vasilev, Surface morphology in the early stages of plasma polymer film growth from amine-containing monomers, Plasma Processes Polym. 8 (2011) 367-372.

[23] S. Schlögl, R. Kramer, D. Lenko, H. Schröttner, R. Schaller, A. Holzner, W. Kern, Fluorination of elastomer materials, Eur. Polym. J. 47 (2011) 2321-2330.

[24] J.H. Yim, V. Rodriguez-Santiago, A.A. Williams, T. Gougousi, D.D. Pappas, J.K. Hirvonen, Atmospheric pressure plasma enhanced chemical vapor deposition of hydrophobic coatings using fluorine-based liquid precursors, Surf. Coat. Technol. 234 (2013) 21-32.

[25] J. Kim, P. Seidler, L.S. Wan, C. Fill, Formation, structure, and reactivity of amino-terminated organic films on silicon substrates, J. Colloid Interface Sci. 329 (2009) 114-119.

[26] M. Pantoja, N. Encinas, J. Abenojar, M.A. Martínez, Effect of tetraethoxysilane coating on the improvement of plasma treated polypropylene adhesion, Appl. Surf. Sci. 280 (2013) 850-857.

[27] C. Li, C. Tu, J. Huang, Y. Liu, K. Lee, J. Lai, Surface modification and adhesion improvement of expanded poly(tetrafluoroethylene) films by plasma graft polymerization, Surf. Coat. Technol. 201 (2006) 63-72.

[28] D. Duday, C. Vreuls, M. Moreno, G. Frache, N.D. Boscher, G. Zocchi, C. Archambeau, C. Van De Weerdt, J. Martial, P. Choquet, Atmospheric pressure plasma modified surfaces for immobilization of antimicrobial nisin peptides, Surf. Coat. Technol. 218 (2013) 152-161.

[29] N. Encinas, B. Díaz-Benito, J. Abenojar, M.A. Martínez, Extreme durability of wettability changes on polyolefin surfaces by atmospheric pressure plasma torch, Surf. Coat. Technol. 205 (2010) 396-402.

[30] N. Encinas, J. Abenojar, M.A. Martínez, Development of improved polypropylene adhesive bonding by abrasion and atmospheric plasma surface modifications, Int.J. Adhes. Adhes. 33 (2012) 1-6.

[31] J. Wang, X. Song, R. Li, J. Shen, G. Yang, H. Huang, Fluorocarbon thin film with superhydrophobic property prepared by pyrolysis of hexafluoropropylene oxide, Appl. Surf. Sci. 258 (2012) 9782-9785.

[32] Y. Chen, H. Kim, Preparation of superhydrophobic membranes by electrospinning of fluorinated silane functionalized poly(vinylidene fluoride, Appl. Surf. Sci. 255 (2009) 7073-7077.

[33] L. Li, F.T. Zi, Y.F. Zheng, The characterization of fluorocarbon films on NiTi alloy by magnetron sputtering, Appl. Surf. Sci. 255 (2008) 432-434.

[34] R. Prikryl, V. Cech, R. Balkova, J. Vanek, Functional interlayers in multiphase materials, Surf. Coat. Technol. 173-174 (2003) 858-862.

[35] C. Kang, H. Lu, S. Yuan, D. Hong, K. Yan, B. Liang, Superhydrophilicity/superhydrophobicity of nickel micro-arrays fabricated by electroless deposition on an etched porous aluminum template, Chem. Eng. J. 203 (2012) 1-8.

[36] Y. Lin, M. Weng, T. Chung, C. Huang, Enhanced surface hardness of flexible polycarbonate substrates using plasma-polymerized organosilicon oxynitride films by air plasma jet under atmospheric pressure, Surf. Coat. Technol. 205 (2011) 3856-3864.

[37] A.J. Choudhury, S.A. Barve, J. Chutia, A.R. Pal, R. Kishore, Jagannath, M. Pande, D.S. Patil, RF-RACVD of water repellent and protective HMDSO coatings on bell metal surfaces: correlation between discharge parameters and films properties, Appl. Surf. Sci. 257 (2011) 8469-8477.

[38] S. Kirk, M. Strobel, C-Y. Lee, S.J. Pachuta, M. Prokosch, H. Lechuga, M.E. Jones, C.S. Lyons, S. Degner, Y. Yang, M.J. Kushner, Fluorine Plasma Treatments of Polyproplylene Films, 1- Surface Characterization, Plasma Processes Polym. 7 (2010) 107-122.

[39] M. Strobel, C.S. Lyons, An Essay on Contact Angle Measurements, Plasma Processes Polym. 8 (2011) 8-13.

[40] H. Unal, U. Sen, A. Mimaroglu, Dry sliding wear characteristics of some industrial polymers against steel counterface, Tribol. Int. 37 (2004) 727-732.

[41] S. Thongsang, W. Vorakhan, E. Wimomala, N. Sombatsompop, Dynamic mechanical analysis and tribological properties of NR vulcanizates with fly ash/precipitated silica hybrid filler, Tribol. Int. 53 (2012) 134-141.

LIST OF FIGURE CAPTIONS

Fig. 1. Chemical structures of the precursors: (a) aminopropyltriethoxysilane (APTES) and (b) (heptadecafluoro-1,1,2,2-tetrahydrodecyl)trimethoxysilane (FLUSI).

(a) CH_3CH_2O, $CH_2CH_2CH_2NH_2$, Si, CH_3CH_2O, OCH_2CH_3

(b) $CF_3(CF_2)_7CH_2CH_2$–Si(–OCH_3)(–OCH_3)(–OCH_3)

Fig 2. Thickness and roughness of all coated samples as a function of the APTES percentage.

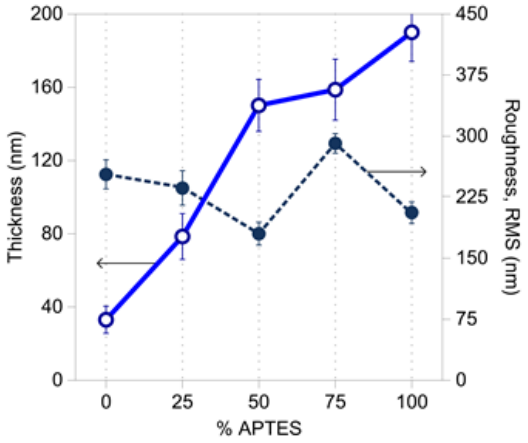

Fig. 3. SEM images of the surface of (a, b) uncoated TPE and coated samples: (c, d) AF_{50}, (e, f) AF_{75} and (g, h) A_{100} at magnifications of x1000 and x5000 respectively. White arrows indicate the location of surface cracks and white circles indicate particles in the coatings.

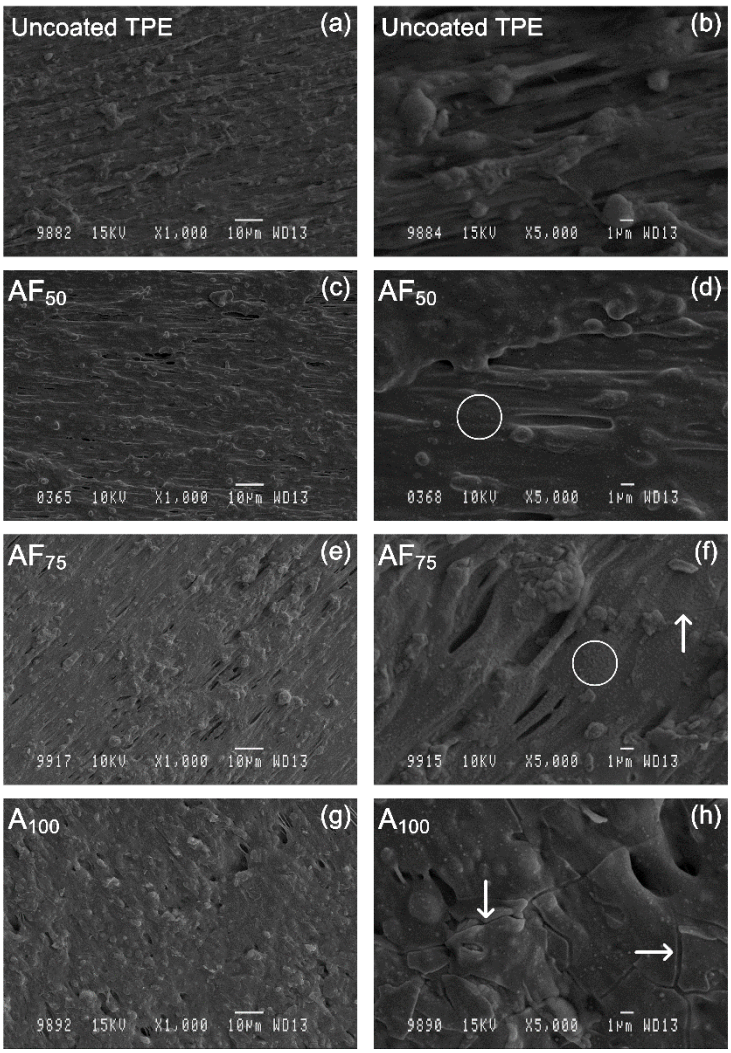

Fig. 4. ATR-FTIR spectrums (600-4000 cm^{-1}) of uncoated TPE and coated samples. The spectrums are displaced from their expected locations by an equal amount of absorbance for purposes of clarity.

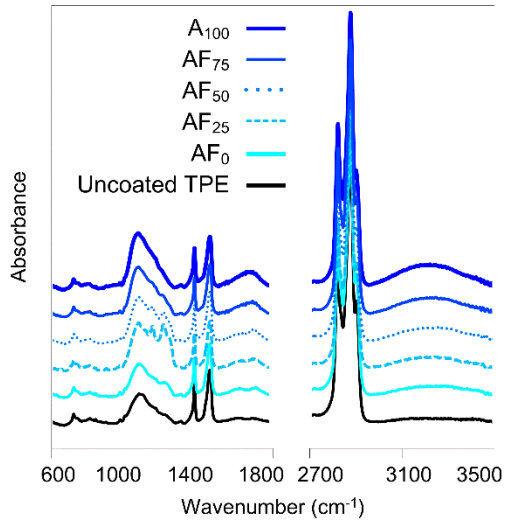

Fig. 5. ATR-FTIR spectrums of the Regions: (I) 980-1280, (II) 1500-1800 and (III) 3000-3700 cm^{-1} of uncoated TPE and coated samples without any displacement.

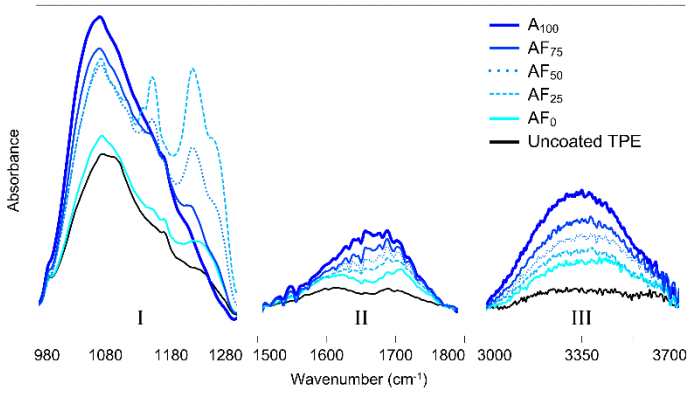

Fig. 6. ATR-FTIR deconvoluted spectrums of Region (I) of uncoated TPE and coated samples.

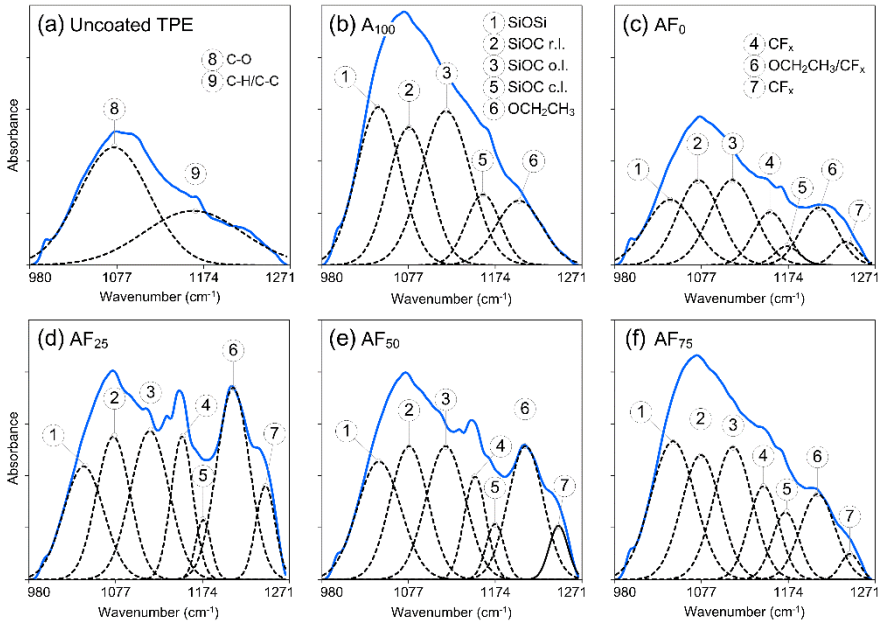

Fig. 7. ATR-FTIR deconvoluted spectrums of Region (II) of uncoated TPE and coated samples.

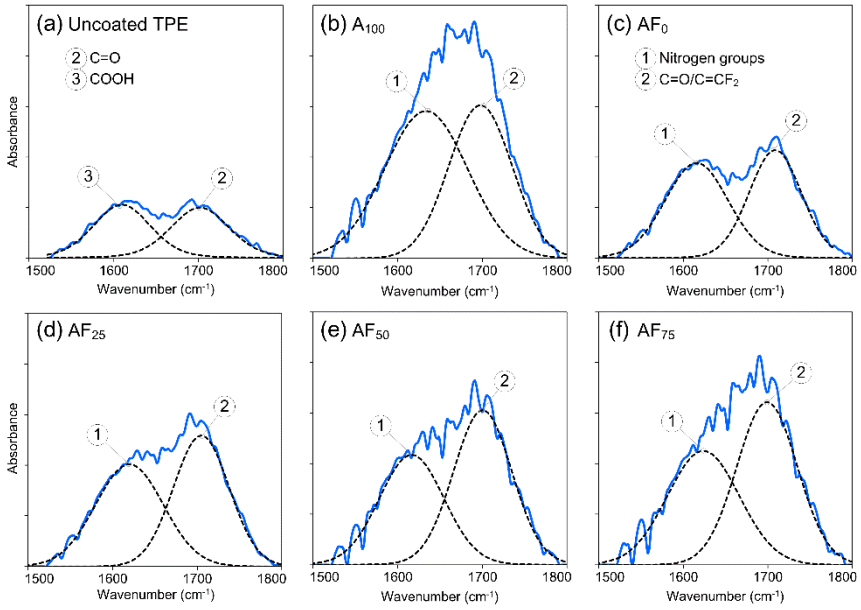

Fig. 8. The absorption areas under the peak of: (a) SiOSi and CF_x, (b) C=O/C=CF_2 and N-groups and (c) OH/NH of coated samples.

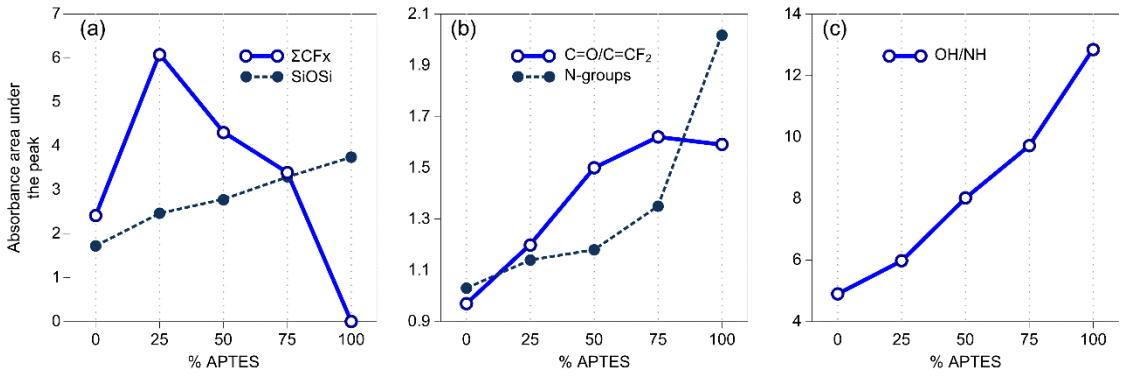

Fig. 9. Atomic compositions (at.%) of the coated samples as a function of the APTES percentage.

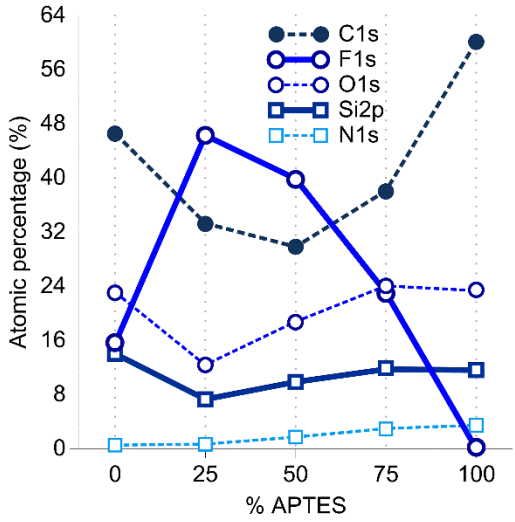

Fig. 10. Deconvolution of high resolution C1s spectrums of all samples.

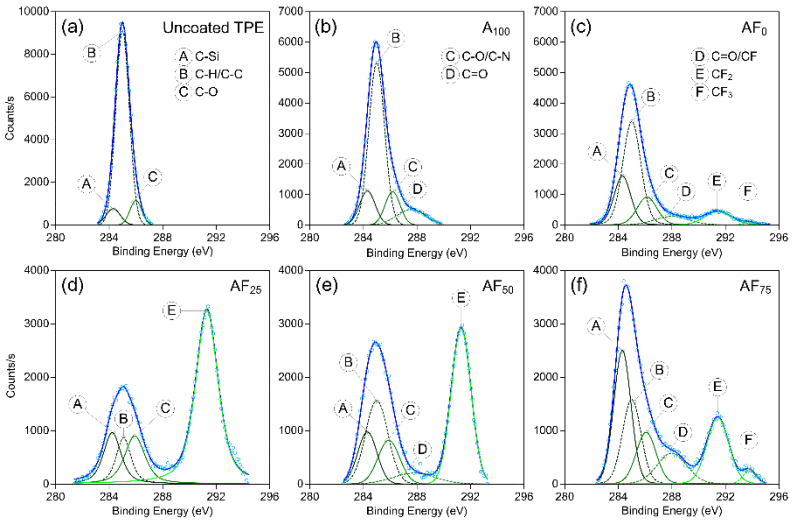

Fig. 11. Relative percentages of chemical bonds: (a) C=O/CF, CF_2 and CF_3 and (b) $(CH_3)_3SiO$, $(CH_3)_2SiO_2$, CH_3SiO_3, SiO_4 and their accumulated proportions of the coated samples.

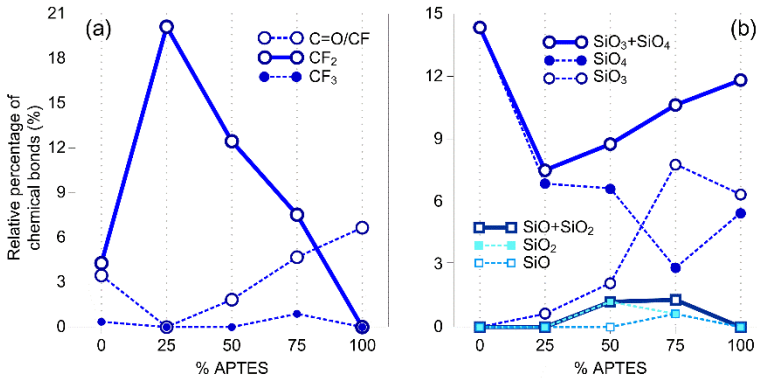

Fig. 12. Deconvolution of high resolution Si2p spectra of all samples.

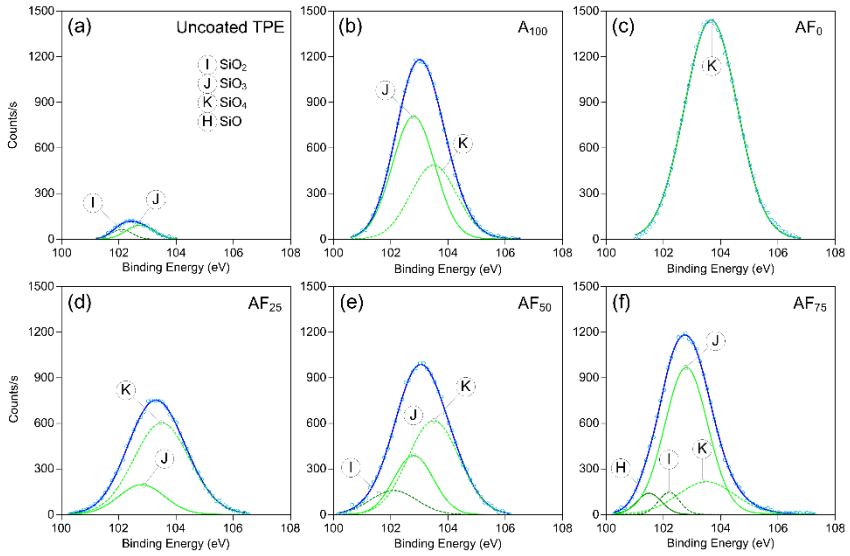

Fig. 13. Advancing (Adv) and Receding (Rec) WCA measurements, the relative percentage of CF_2 and the relative percentage of polar groups of the coated samples as a function of the APTES percentage.

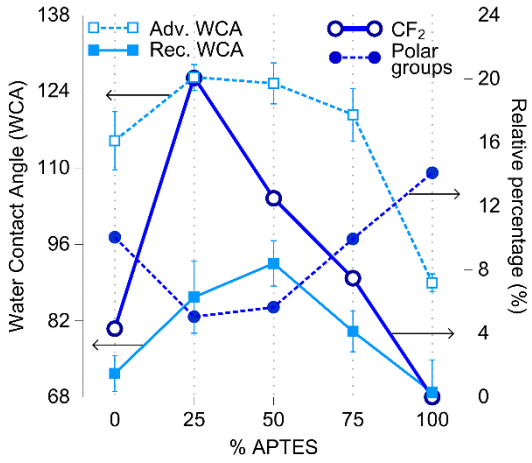

Fig 14. ATR-FTIR of uncoated TPE, AF_{25} and AF_{75} samples at the beginning and upon completion of the stability test.

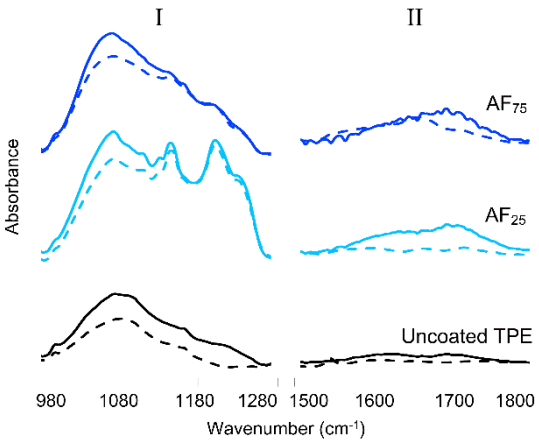

Fig. 15. Static WCA of all the studied samples at the beginning and upon completion of the stability tests.

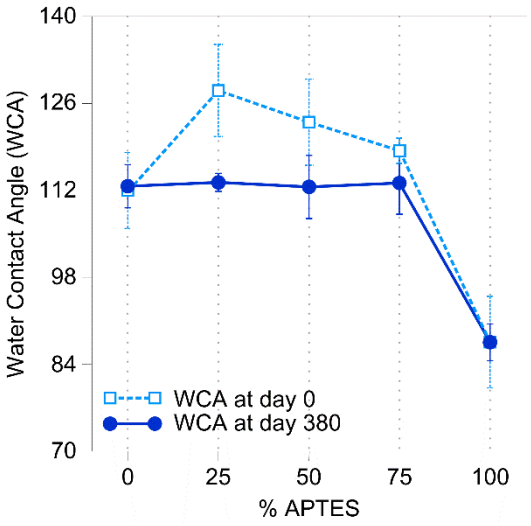

Fig. 16. Friction coefficient of all samples tested with a steel ball.

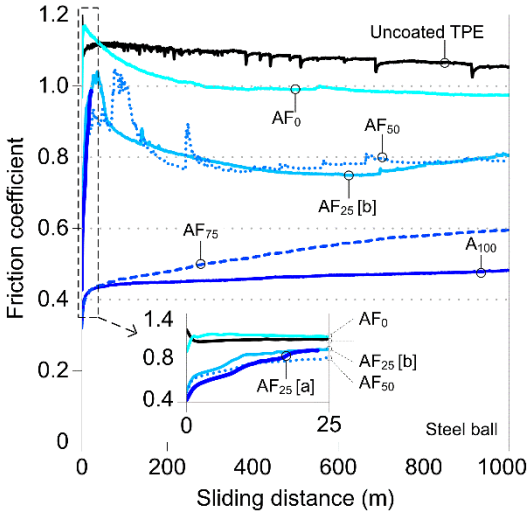

Fig. 17. SEM images from the wear tracks at different magnification (x 80 and x 600) of samples: (a) and (b) Uncoated TPE, (c), (d), (e) and (f) AF_{25} and (g) A_{100}. Images (a), (b), (e), (f) and (g) at a sliding distance of 1000 m and (c) and (d) at a sliding distance of 22 m. The tests were done with a steel ball.

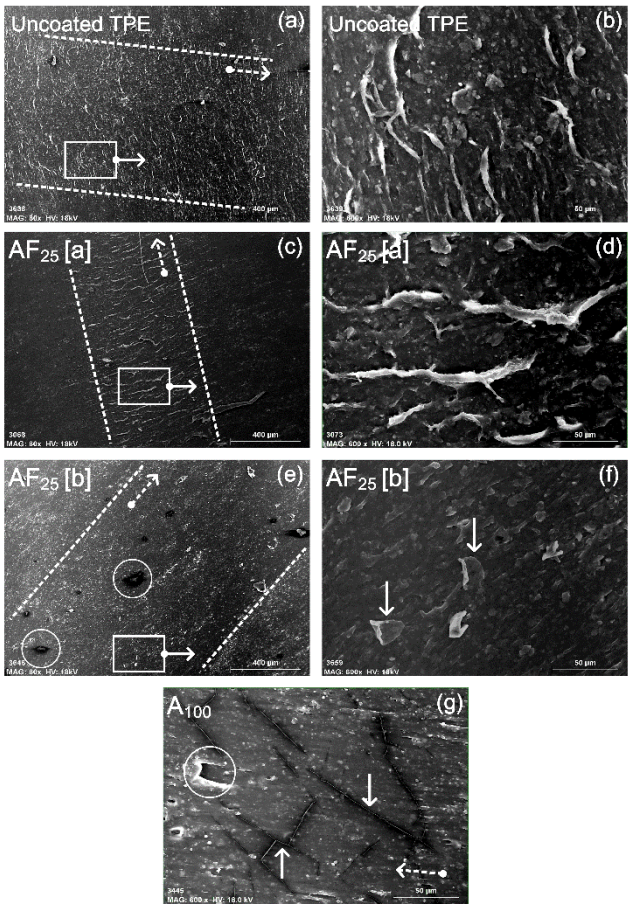

Fig. 18. Friction coefficient of all samples tested with a glass ball.

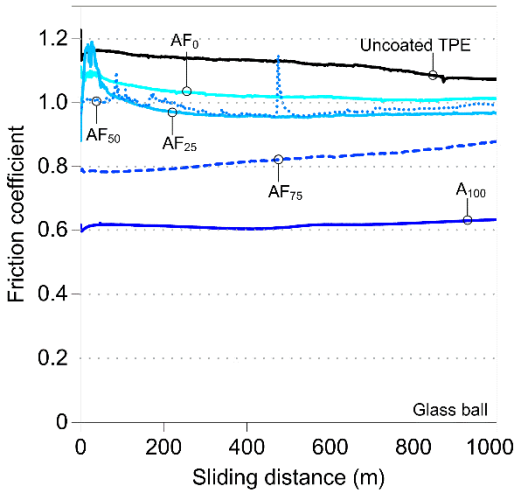

Fig. 19. (a) The absorbance area under the peak of SiOSi, (b) the relative percentage of inorganic groups, (c) the relative percentage of CF_2 groups, (d) the relative percentage of polar groups and (e) the average friction coefficient and advancing WCA of coated samples.

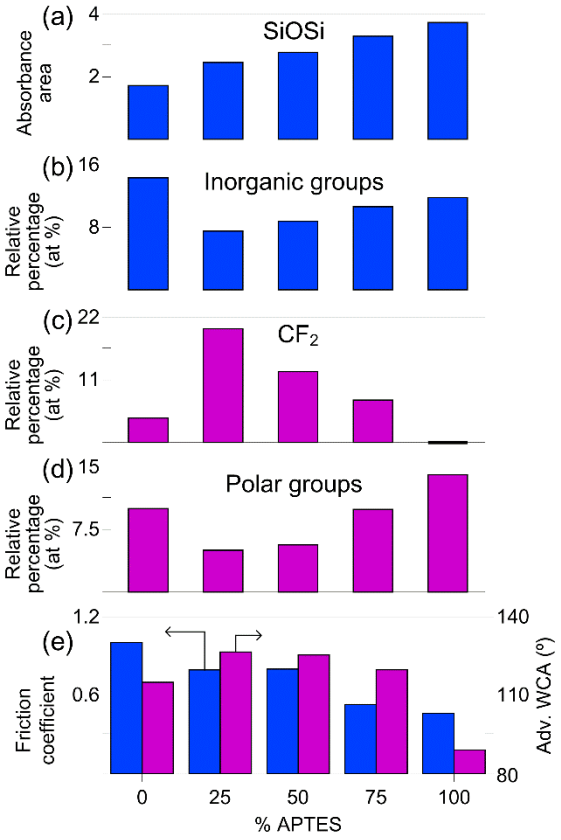

LIST OF TABLE CAPTIONS

Table. 1. Label of each sample according to the percentages of APTES and FLUSI in the precursor mixture.

Sample label	Precursor (%)	
	APTES	FLUSI
AF_0	0	100
AF_{25}	25	75
AF_{50}	50	50
AF_{75}	75	25
A_{100}	100	0
Uncoated TPE	0	0

Table. 2. Process parameters for plasma deposition by APPJ.

Parameter	Setting
Plasma power (W)	450
Frequency (kHz)	75
Ionization gas flow (N_2)	80 slm
Precursor flow rate	1.5 slm
Gun speed (m/min)	6
Track pitch (mm)	2
Gap distance (mm)	6

Table. 3. Assigned chemical components and peak position in deconvoluted high resolution C1s and Si2p spectrums.

	Component	Chemical components	Peak position (eV)	References
C1s	A	C-Si	~284.3	[24,35]
	B	C-C C-H	~285	[21,24,28,35]
	C	C-N C-O	~286	[17,24,26,28]
	D	C=O CF	~288	[21,26,28]
	E	CF_2	~291.4	[21,24]
	F	CF_3	~293.8	[14,21,24,35]
Si2p	G	$(CH_3)_4Si$	~100.9	[36]
	H	$(CH_3)_3SiO$	~101.5	[36]
	I	$(CH_3)_2SiO_2$	~102.1	[36]
	J	CH_3SiO_3	~102.8	[36]
	K	SiO_4	~103.4	[36]

Table 4. Average friction coefficient of all samples with both the steel ball and the glass ball as counterpart.

Sample label	Steel ball as counterpart			Glass ball as counterpart
	Total sliding distance (meters)	Average friction coefficient	Maximum friction coefficient (at sliding distance in meters)	Average friction coefficient
Uncoated TPE	1000	1.084 ± 0.019	1.22 (0)	1.120 ± 0.026
AF_0	1000	1.006 ± 0.072	1.16 (8)	1.025 ± 0.021
AF_{25} [a]	22	0.701 ± 0.058	0.99 (22)	0.974 ± 0.038
AF_{25} [b]	1000	0.796 ± 0.055	1.05 (36)	-
AF_{50}	1000	0.802 ± 0.056	1.05 (77)	0.982 ± 0.021
AF_{75}	1000	0.530 ± 0.050	0.60 (996)	0.822 ± 0.027
A_{100}	1000	0.461 ± 0.015	0.48 (996)	0.616 ± 0.008